



Article

Stress Dispersion Design in Continuum Compliant Structure toward Multi-DOF Endoluminal Forceps

Keisuke Osawa ^{1,*}, D. S. V. Bandara ¹, Ryu Nakadate ² , Yoshihiro Nagao ³, Tomohiko Akahoshi ⁴, Masatoshi Eto ⁵  and Jumpei Arata ¹

¹ Department of Mechanical Engineering, Faculty of Engineering, Kyushu University, Fukuoka 819-0395, Japan; d-sanjaya@mech.kyushu-u.ac.jp (D.S.V.B.); jumpei@mech.kyushu-u.ac.jp (J.A.)

² Center for Advanced Medical Innovation, Kyushu University, Fukuoka 812-8582, Japan; nakadate@camiku.kyushu-u.ac.jp

³ Department of Advanced Medicine and Innovative Technology, Kyushu University Hospital, Fukuoka 812-8582, Japan; nagao.yoshihiro.796@m.kyushu-u.ac.jp

⁴ Department of Advanced Medical Initiatives, Graduate School of Medical Science, Kyushu University, Fukuoka 812-8582, Japan; akahoshi.tomohiko.006@m.kyushu-u.ac.jp

⁵ Department of Urology, Graduate School of Medical Sciences, Kyushu University, Fukuoka 812-8582, Japan; etom@uro.med.kyushu-u.ac.jp

* Correspondence: osawa@amd.mech.kyushu-u.ac.jp

Abstract: Gastrointestinal cancer, when detected early, is treated by accessing the lesion through the natural orifice using flexible endoscopes. However, the limited degree-of-freedom (DOF) of conventional treatment devices and the narrow surgical view through the endoscope demand advanced techniques. In contrast, multi-DOF forceps systems are an excellent alternative; however, these systems often involve high fabrication costs because they require a large number of micro-parts. To solve this problem, we designed compact multi-DOF endoluminal forceps with a monolithic structure comprising compliant hinges. To allow an efficient stress dispersion at the base end when the hinge bends, we proposed a novel design method to obtain the hinge parameters using the beam of uniform strength theory. This method does not involve a high computational cost. The results show that the improved design with a variable hinge thickness can reduce the maximum bending stress, dispersing the stress in a larger area than that of the previous design considering a constant thickness of the hinge. Moreover, the experiments conducted in a prototype confirm that the radius of the curvature was significantly improved. The proposed method could aid in designing other continuum robots relying on compliant hinges.

Keywords: design methodology; finite element analysis; medical robotics; surgical instruments; soft robotics



Citation: Osawa, K.; Bandara, D.S.V.; Nakadate, R.; Nagao, Y.; Akahoshi, T.; Eto, M.; Arata, J. Stress Dispersion Design in Continuum Compliant Structure Toward Multi-DOF Endoluminal Forceps. *Appl. Sci.* **2022**, *12*, 2480. <https://doi.org/10.3390/app12052480>

Academic Editor: Byung-Ju Yi

Received: 12 January 2022

Accepted: 23 February 2022

Published: 27 February 2022

Publisher's Note: MDPI stays neutral with regard to jurisdictional claims in published maps and institutional affiliations.



Copyright: © 2022 by the authors. Licensee MDPI, Basel, Switzerland. This article is an open access article distributed under the terms and conditions of the Creative Commons Attribution (CC BY) license (<https://creativecommons.org/licenses/by/4.0/>).

1. Introduction

Advances in endoscopic equipment have enabled early diagnosis and minimally invasive resection of esophageal, gastric, and colorectal cancers. In particular, endoscopic submucosal dissection (ESD) is an advanced method that allows setting an arbitrary excision range. Moreover, ESD enables the accurate excising of larger lesions than other procedures [1,2]. However, ESD is a time-consuming and challenging procedure. The risk of bleeding or perforation with a slight operation error is present. Specifically, in cases where the submucosa is not completely visible, the submucosal dissection is challenging. A good field of view with counter traction can facilitate and save the ESD procedure [3,4]. In this regard, articulated forceps are effective in obtaining adequate traction.

Previous studies have developed multi-DOF endoluminal forceps with articulated joint structures [5–19]. For instance, Anubiscope [5], STRAS [6], EndoMaster [7], and K-FLEX [8] have improved workability. Their effectiveness has been demonstrated by performing ESD procedures using a porcine stomach and colon and comparing specimen

size and dissection speed. Similarly, *i² Snake* [9], EndoSamurai [10], ViaCath [11], and Flex robotic system [12] are endoscopic surgical systems for natural orifice transluminal endoscopic surgery (NOTES) or other endoscopic surgery. These devices [5–12] are equipped with articulating segments. However, their diameters are not sufficiently small to be inserted into the 2.8 mm channel of commercially available prevailing standard flexible endoscopes. Other articulated devices [13–19] are within 2.6 mm in diameter. Thus, these devices might be used with standard flexible endoscopes even though each mechanism has its own limitations. Lee et al.'s [13] and Kawahara et al.'s [14] devices have only one-DOF of bending. Prasai et al.'s [15] device has a problem that the bending radius becomes large because it is bent by rotating a multi-layered concentric tube. Nakadate et al.'s [16–18] and Ray et al.'s [19] mechanisms contain several micro-parts, which increases their cost. Considering size and cost, a mechanism with the simplest possible structure is desirable.

Therefore, we designed a multi-DOF monolithic-structured forceps within 2.6 mm in diameter. The designed forceps have a compact configuration composed of a grasping segment, bending segment, and tendon-sheath driving segment. The grasping and bending segments have a monolithic structure relying on a compliant mechanism [20], which is a flexible mechanism achieving force and motion transmission through elastic body deformation. The compliant mechanism has the advantages of being integrally molded with a smaller size, lighter weight, and simpler structure than conventional mechanisms. However, when a compliant joint bends, the stress generally concentrates at the end of the base, placing heavy loads on the first few joints, leading to fatigue failure. This limits the range of motion of the mechanism and is a typical inconvenience of continuum robots using similar compliant joints [21–23].

In this regard, some studies have used FEA to improve the design of the joint structures [24–27]. For instance, Park et al. [24] and Wu et al. [25] evaluated the design optimization by changing the thickness of the hinge using FEA. Huang et al. [26] studied the structural behavior of the snake-like mechanism depending on the dimensions of individual joints and sought to achieve a particular curvature. Furthermore, the thickness of the hinge varies along the structure. Coemert et al. [27] presented the design optimizations by changing the thickness of the hinge for each segment using FEA to adjust a uniform stress distribution. The design optimization approach was validated using a 1-DOF compliant joint with three segments of elastic hinges. However, in these studies [24–27], a problem arose regarding the high computational cost due to the nonlinear analysis with fine mesh and the exploratory thickness determination of elastic hinges.

In this study, we propose a novel method to efficiently determine the thickness of the elastic hinges by modeling the stress distribution mathematically using the theory of the beam of uniform strength [28]. In particular, the technical contributions of this paper are: (1) A novel design method was proposed to determine the thickness of continuum hinges based on the beam of uniform strength theory. (2) Endoluminal forceps were developed with a wide range of motion and a small radius of curvature even in a narrow lumen due to the stress dispersion design method.

This paper is organized as follows: Section 2.1 presents the mechanical structure of the designed forceps. Section 2.2 describes the design method for obtaining the new hinge parameters. The section is followed by the stress evaluation through FEA presented in Section 3.1. In Section 3.2, a prototype is used to compare the differences in motion generation between the variable thickness of the hinge and the constant thickness of the hinge. Section 4 discusses the results, as well as the study's contributions and limitations. Finally, Section 5 provides the conclusions.

2. Stress Dispersion Design Method

The proposed design method aims to reduce stress concentration at the end of the base while ensuring a wide range of motion.

2.1. Basic Design

The developed forceps structure consists of three segments: grasping, bending, and driving, as shown in Figure 1. Although the grasping and bending segments are monolithically structured, these segments provide 3-DOF, with 2-DOF of bending and grasping through a tendon-sheath mechanism. A single-piece construction prevents losing parts in the operation. In particular, the grasping segment has an outer diameter of 2.5 mm in the proposed design. Moreover, the bending segment has an outer diameter of 2.3 mm because the outer peripheral surface is assumed to be covered with a heat-shrinkable tube. The driving segment has a compact structure consisting of five wires with an outer diameter of 0.3 mm and five tubes with an outer diameter of 0.6 mm. The wires are driving using servo motors or a connected mechanical joystick. When tension is applied to the center wire, the driving force transmission part is deformed in the loading direction, the side surface part elastically deforms, and the tip opens and closes. The bending uses an antagonistic drive method that bends up, down, left, and right through four wires. When tension is applied to the wire, a bending moment is applied to the tip, deforming the continuous hinges to bend.

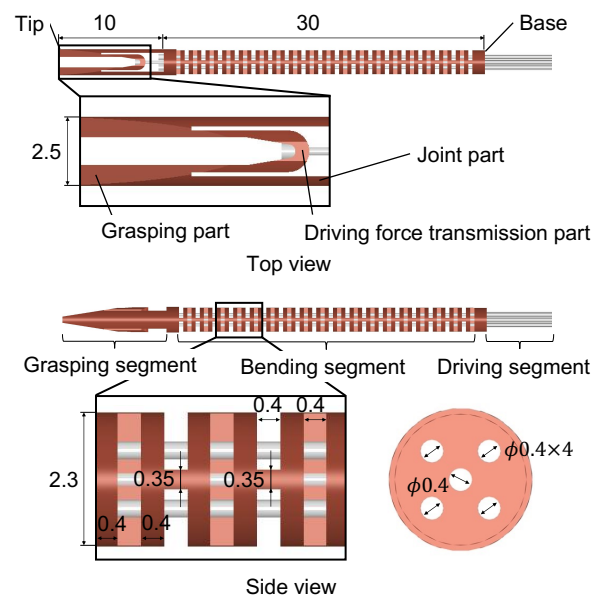
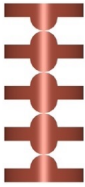



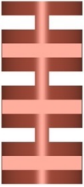



Figure 1. Structure of the designed forceps.

Several studies [29–50] have introduced continuum robots using hinge designs. As shown in Table 1, the hinge design can be classified into several types: (i) discrete joint [29–31], (ii) uni-directional compliant joint [32–35], (iii) bi-directional compliant joint [36–41], (iv) cross-axis compliant joint [42,43], (v) helical compliant joint [44–46], and (vi) symmetric compliant joint [47–50]. We selected a symmetric compliant joint, which has the advantage of high flexibility and strength for grasping and bending. By using elastic deformation, the mechanism could be operated without mechanical backlash.

Table 1. Classification of several hinge types in related studies: (i) discrete joint, (ii) uni-directional compliant joint, (iii) bi-directional compliant joint, (iv) cross-axis compliant joint, (v) helical compliant joint, and (vi) symmetric compliant joint.

						
	i.	ii.	iii.	iv.	v.	vi.
Classification	Discrete joint	Uni-directional compliant joint	Bi-directional compliant joint	Cross-axis compliant joint	Helical compliant joint	Symmetric compliant joint
Parts of joint	Discrete	Compliant	Compliant	Compliant	Compliant	Compliant
Symmetry	Symmetric	Asymmetric	Asymmetric	Asymmetric	Asymmetric	Symmetric
Direction of bending	Bi-directional	Uni-directional	Bi-directional	Bi-directional	Bi-directional	Bi-directional
DOF of bending	1-DOF	1-DOF	1-DOF	1-DOF	2-DOF	2-DOF
Advantage	Wide range of motion	Compact flexure, low stress	Compact flexure, low stress	Compact flexure	Low stress	High flexibility and strength
Disadvantage	High assembly cost	Longer segment with 2-DOF	Long segment with 2-DOF	Complex structure	Low position accuracy	High stress
Reference	[29–31]	[32–35]	[36–41]	[42,43]	[44–46]	[47–50]

2.2. Design Improvement

A beam of uniform strength is a beam whose bending stress is constant in the longitudinal direction of the beam. For example, when considering a cantilever beam that receives a concentrated load on the tip, the bending moment acting on the beam increases proportionally to the distance from the tip. Therefore, if the cross-section is uniform, the magnitude of bending stress is also proportional to the distance tip and becomes maximum at the fixed end. If a beam is designed so that the section modulus increases proportionally to the distance from the tip, the bending stress becomes constant regardless of the position. In contrast, no straightforward method exists to determine the hinge size to distribute the stress effectively because the designed forceps relies on a discontinuous beam. In this study, we propose a method to effectively determine the parameters by using the beam of uniform strength concept.

That is, assume a concentrated load P acting on the free end of the cantilever shown in Figure 2, where x is the arbitrary position in the length direction. The cross-sectional shape is a rectangle with a width of b and a thickness of h_x at an arbitrary position in the length direction. h_0 is the thickness at $x = l$. When b is constant, h_x becomes parabolic [51]. The applied moment M and the section modulus Z are expressed as follows:

$$M = Px, Z = \frac{bh_x^2}{6} \quad (1)$$

Thus, the maximum bending stress σ_{max} is expressed as follows:

$$\sigma_{x(max)} = \frac{M}{Z} = \frac{6Px}{bh_x^2} \quad (2)$$

$$\sigma_{l(max)} = \frac{6Pl}{bh_0^2} \quad (3)$$

where $\sigma_{x(max)}$ and $\sigma_{l(max)}$ are the maximum bending stress at an arbitrary position in the length direction and the base end, respectively. Considering a beam of uniform strength, $\sigma_{x(max)} = \sigma_{l(max)}$. Therefore,

$$\sigma_{x(max)} = \frac{6Px}{bh_x^2} = \frac{6Pl}{bh_0^2} \quad (4)$$

$$h_x = h_0 \sqrt{\frac{x}{l}} \quad (5)$$

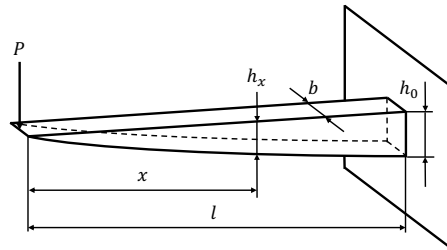


Figure 2. Diagram of beam of uniform strength.

Due to the size limitations of the endoluminal forceps, $h_0 = 0.6$ mm, $l = 30$ mm. By substituting these parameters into Equation (5), the thickness of the beam of uniform strength can be calculated. The hinge thickness was determined according to the thickness for each length of the beam of uniform strength. In the proposed method, average thicknesses of two pairs of adjacent hinges are matched with thickness of beam of uniform strength. The thicknesses for each position in the length direction of beam of uniform strength, initial design, and improved design are shown in Figure 3. The hinge lengths were designed as (a) 0.2 mm, (b) 0.4 mm, (c) 0.8 mm, and (d) 1.2 mm. Figure 4 shows the initial and improved designs with the 0.4 mm length hinge.

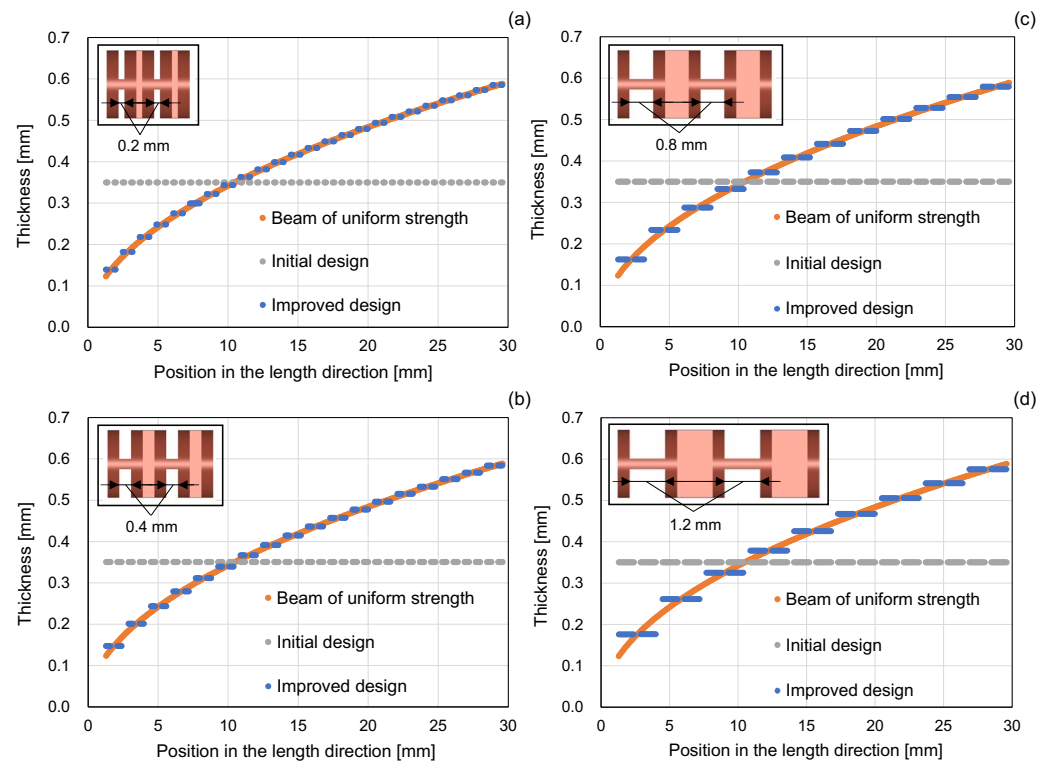


Figure 3. Thicknesses (beam of uniform strength, initial design, improved design) for each hinge length: (a) 0.2 mm, (b) 0.4 mm, (c) 0.8 mm, and (d) 1.2 mm.

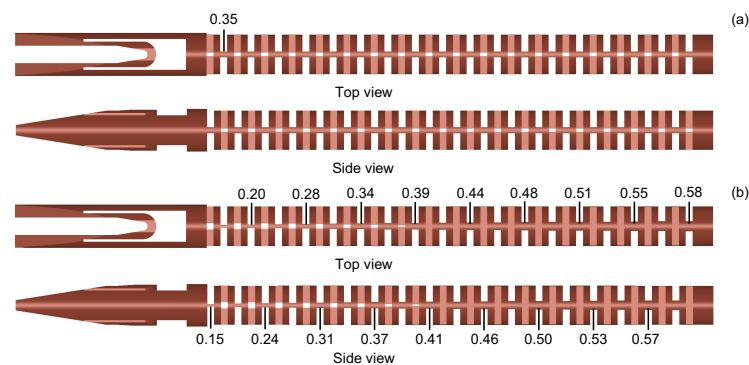


Figure 4. Diagram of the forceps when the hinge length was 0.4 mm: (a) initial design and (b) improved design.

3. Evaluation

The proposed design was evaluated using FEA and an experimental prototype to confirm the effectiveness of the proposed stress dispersion design method.

3.1. Finite Element Analysis

FEA was used to quantitatively evaluate the stress distribution to analyze whether a reduction in the stress concentration was achieved. Initially, we determined the material and FEA conditions. Polymer materials can be mass-produced at a low cost and discarded after one-time use. PAI (Polyamide-imide) is a biocompatible material with a low Young's modulus and yield strength among similar polymer materials [24]. Therefore, PAI is suitable as a material for the hinge of the forceps. In particular, FEMAP (SIEMENS PLM, Stuttgart, Germany) was used to generate the mesh considering tetrahedral elements. The analyses were conducted using the nonlinear numerical-analysis software DAFUL (Virtual Motion, Seoul, Korea). Table 2 shows the physical properties of PAI and the mesh size used for FEA. To be able to operate the forceps like a human wrist, the required range of motion is ± 90 degrees. Therefore, the force applied until the forceps bent 90 degrees in FEA. The FEA considered that the tensile force was always perpendicular to the tip of the surface each time the tip bent. First, a simulation was performed where a wire was pulled and bent in a lateral direction. Subsequently, a simulation was performed where two wires were pulled and bent in an oblique direction. The analysis conditions were set so that the tensions of the two wires were equal. To show the effectiveness of the improved design with a variable hinge thickness, we compared it to an initial design with a constant hinge thickness. For the design used for comparison, only the hinge size was changed, and the other parameters were maintained of the same size. The hinge thickness of the initial design was 0.35 mm.

Table 2. Material properties and mesh size considered in the FEA.

Material Property	Value
Young's modulus	4000 (MPa)
Shearing modulus	1379 (MPa)
Yield strength	152 (MPa)
Poisson ratio	0.45
Mesh size	0.15 (mm)

The FEA results when the hinge length was 0.4 mm are shown in Figure 5. Figure 6 shows the evenly distributed stress when the hinge length was 0.4 mm. When the tip was bent 90 degrees, the maximum stress of the initial design and improved design was 245 MPa and 148 MPa, respectively. Consequently, the maximum stress is smaller than the yield strength of PAI. The improved design allowed stress dispersion, and the maximum

stress was substantially reduced compared to that of the initial design. Figure 7 shows the results of comparing the maximum stresses when FEA is performed using different hinge lengths. For all hinge lengths, the improved design significantly reduced the maximum stress compared to the initial design. However, the maximum bending stresses of the initial design and the improved design are larger than the yield stress of PAI when pulling with two wires. Therefore, the angle at the maximum bending stress that does not exceed the yield stress is defined as the maximum bending angle, as shown in Figure 7. The bending range of the improved design was larger than that of the initial design. Note that the average analysis time for non-linear analysis using FEA required approximately 4800 s on a computer with an Intel Xeon W-3235 Deca-core 3.30 GHz, using 192 GB of RAM. The proposed method can derive parameters in almost real time, even using versatile numerical calculation software. Thus, the proposed method obtained the design parameters with a lower computational cost than the design method of previous research using FEA [24–27]. The results show the effectiveness of the proposed design method for successful motion generation.

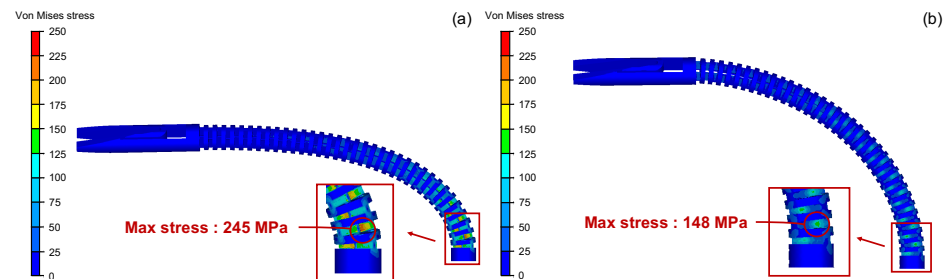


Figure 5. FEA results when the hinge length was 0.4 mm: (a) initial design and (b) improved design.

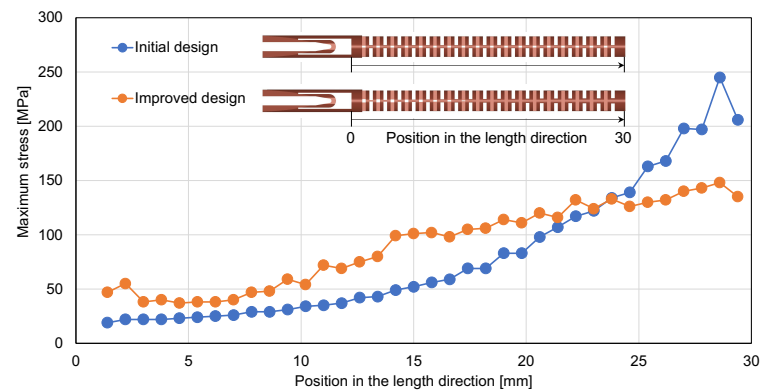


Figure 6. Distribution of maximum stress for each segment when the hinge length was 0.4 mm.

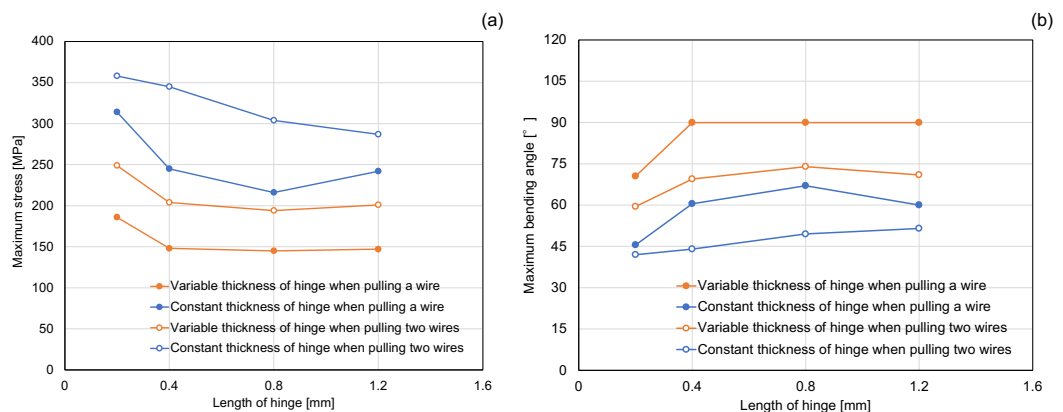


Figure 7. FEA results of the initial and improved designs for each hinge length: (a) maximum stress and (b) maximum bending angle.

3.2. Prototype Experiment

This experiment aimed to validate the effectiveness of the proposed design method by performing motion generation using a prototype. Similar to the FEA results, the experiments confirmed that the smaller the radius of curvature, the more the stress can be dispersed at the base end. Therefore, the radii of curvature of the improved design and the initial design were compared as evaluation indexes. A 3D printer (Objet30, Stratasys, Eden Prairie, MN, USA) was used to ensure rapid prototyping. The material of the 3D printer was the acrylic resin Verowhite. This material will be replaced by biocompatible materials such as PAI in the future. The experiments considered motion generation by pulling a prototype fixed to a jig using an electric measuring stand (EMX-1000N, IMADA, Toyohashi, Japan) and a force gauge (ZTA-5N, IMADA, Toyohashi, Japan) with a stainless wire with an outer diameter of 0.3 mm. The prototype was printed together with the jig to provide stable fixation for the measurements. This approach prevented the fixed end from shifting or tilting. The hinge length was set to 0.4 mm, and other parameters were the same as the design used in FEA. The outline of this experiment is shown in Figure 8. The force gauge was varied up and down at a constant speed of 50 mm/min, and tension was applied to the tip of the prototype with a wire. Due to the difficulties in measuring the radius of curvature, we compared the displacement of the tips. The displacement was measured using a motion analyzer (VW-9000, KEYENCE, Osaka, Japan) from a video obtained with a camera. The prototype could bend within a range of 180 degrees. Figure 9 shows the displacement of motion generation using the prototype for each hinge length. The results show that the improved design for each hinge length had a smaller displacement than the initial design. Therefore, the prototype experiments confirmed that the stress was significantly reduced. The results with the fabricated prototype also show the effectiveness of the proposed design method for successful motion generation.

Finally, a feasibility test was conducted to confirm that the mucous membrane could be lifted by the improved forceps. As shown in Figure 10, a pre-cut simulated intestinal four-layered sheet (Kyoto Kagaku, Kyoto, Japan) was successfully lifted by the 3D-printed prototype based on the improved design. Therefore, the result confirmed the feasibility of the improved design.

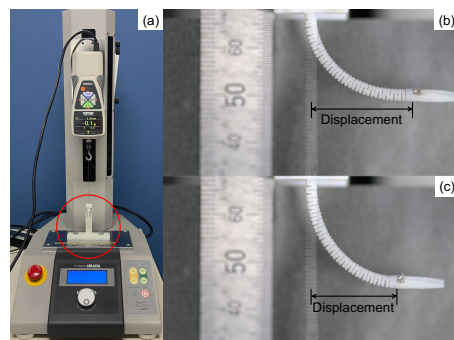


Figure 8. Experimental image of the motion generation using the prototype: (a) experimental setup, (b) initial design, and (c) improved design.

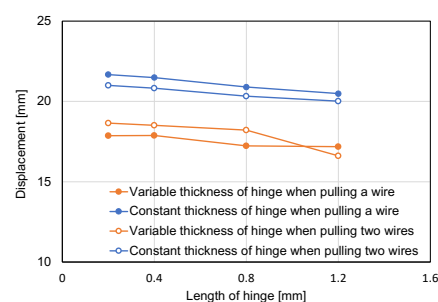


Figure 9. Displacement of the motion generation using the prototype for each hinge length.

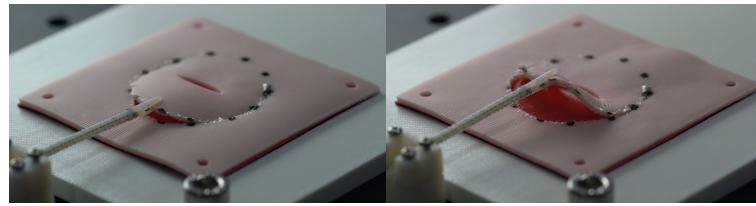


Figure 10. Experimental image of lifting a simulated intestinal sheet using the improved forceps

4. Discussions

The novel design method proposed in this study largely decreased the stress, providing a practical way for designing continuum-compliant structures. Moreover, the proposed method obtained the design parameters at a lower computational cost than FEA. This has been successfully demonstrated in the FEA and the prototype experiment. Nevertheless, some aspects should be discussed.

First, FEA results showed that the maximum bending stress is smaller than the yield strength of PAI. This is a significant achievement, as designing below yield stress in limited sizes and materials with conventional design methods is challenging. However, the same mesh size was applied to verify the effectiveness of the proposed design method using FEA. The validity of the mesh size should be further investigated by performing a mesh sensitivity analysis.

Second, stress evaluation was performed only for wire tension without grasping an object. Therefore, the maximum stress is expected to be higher while holding an object. Further, when lifting a part of the mucous membrane, there is a possibility to cause a large deformation. It should be investigated assuming a clinical application. On the other hand, the proposed method could also be applied to the design improvement of the grasping segment. In addition, the stress concentration at the base end of the bending segment was improved. However, it is necessary to consider compressive stress and rigidity as evaluation indexes.

Third, there is a possibility that an external force may be applied to the forceps in the narrow gastrointestinal tract. This aspect was not considered in this study. Moreover, covering the bending segment with a heat-shrinkable tube might affect the stress dispersion and the radius of curvature.

Finally, the prototype was developed using rapid prototyping with Verowhite. However, the 3D printing method of PAI is typically a fused deposition modeling (FDM) method; thus, this method is not suitable for building micro-parts. In addition, the FEA results and prototype experiments showed similar tendencies but with some errors between each other. There are differences in material properties such as yield stress and elongation between VeroWhite and PAI. Future work should be conducted in these directions.

5. Conclusions

In this study, we proposed a stress-dispersion design method for a multi-DOF continuum-compliant structure. Moreover, its effectiveness in designing endoluminal forceps was verified. The proposed method obtained the hinge thickness according to the thickness of the beam of uniform strength. The improved design dispersed the stress, and the maximum stress was substantially reduced compared to the initial design. Thus, a wide range of motion was achieved. In addition, we experimented with a prototype. The results confirmed that the radius of curvature was significantly improved. The proposed method could be a great advantage for endoluminal procedures in narrow lumens. The findings can be summarized as follows: (1) The proposed design method can efficiently determine the hinge thickness even with different hinge lengths. (2) A stress concentration could be prevented by changing the hinge thickness of each segment for a compliant joint based on the theory of beam of uniform strength. This versatile method could improve the design of other continuum robots relying on compliant hinges.

The proposed design method could be applied to various medical robots. For instance, in the tip bending of catheters and endoscopes, the proposed method could allow low-cost manufacturing with a smaller diameter than the conventional design. Moreover, by applying the proposed method to biomimetic robots, such as snakes and octopuses, it could be possible to enter into narrower spaces by downsizing.

In the future, we will perform the experiments using a porcine stomach and colon. The grasping structure should be further improved. For instance, shape optimization can be performed using methods, such as topology optimization, FEA, and strength of materials. The improved forceps have a wide range of motion with a simple structure and is suitable for mass production. Thus, it can be manufactured at a low cost. Therefore, these forceps have the potential for ESD procedures, NOTES, ERCP (Endoscopic Retrograde Cholangiopancreatography), and endoscopic hemostasis.

Author Contributions: Conceptualization, K.O., D.S.V.B. and J.A.; methodology, K.O.; validation, Y.N., T.A. and M.E.; investigation, K.O. and D.S.V.B.; resources, R.N., Y.N., T.A., M.E. and J.A.; writing—original draft preparation, K.O.; writing—review and editing, D.S.V.B. and J.A.; supervision, J.A.; funding acquisition, J.A. All authors have read and agreed to the published version of the manuscript.

Funding: This research received no external funding.

Institutional Review Board Statement: Not applicable.

Informed Consent Statement: Not applicable.

Data Availability Statement: Not applicable.

Conflicts of Interest: The authors declare no conflict of interest.

References

1. Gotoda, T.; Kondo, H.; Ono, H.; Saito, Y.; Yamaguchi, H.; Saito, D.; Yokota, T. A new endoscopic mucosal resection procedure using an insulation-tipped electrosurgical knife for rectal flat lesions: Report of two cases. *Gastrointest. Endosc.* **1999**, *50*, 560–563. [\[CrossRef\]](#)
2. Yahagi, N.; Fujishiro, M.; Kakushima, N.; Kobayashi, K.; Hashimoto, T.; Oka, M.; Iguchi, M.; Enomoto, S.; Ichinose, M.; Niwa, H.; et al. Endoscopic submucosal dissection for early gastric cancer using the tip of an electrosurgical snare (thin type). *Dig. Endosc.* **2004**, *16*, 34–38. [\[CrossRef\]](#)
3. Deprez, P.H.; Bergman, J.J.; Meisner, S.; Ponchon, T.; Repici, A.; Dinis-Ribeiro, M.; Haringsma, J. Current practice with endoscopic submucosal dissection in Europe: Position statement from a panel of experts. *Endoscopy* **2010**, *42*, 853–858. [\[CrossRef\]](#)
4. Fukamim, N. What we want for ESD is a second hand! Traction method. *Gastrointest. Endosc.* **2013**, *78*, 274–276. [\[CrossRef\]](#) [\[PubMed\]](#)
5. Diana, M.; Chung, H.; Liu, K.H.; Dallemagne, B.; Demartines, N.; Mutter, D.; Marescaux, J. Endoluminal surgical triangulation: Overcoming challenges of colonic endoscopic submucosal dissections using a novel flexible endoscopic surgical platform: Feasibility study in a porcine model. *Surg. Endosc.* **2013**, *27*, 4130–4135. [\[CrossRef\]](#)
6. Zorn, L.; Nageotte, F.; Zanne, P.; Legner, A.; Dallemagne, B.; Marescaux, J.; de Mathelin, M. A novel telemanipulated robotic assistant for surgical endoscopy: Preclinical application to ESD. *IEEE Trans. Biomed. Eng.* **2018**, *65*, 797–808. [\[CrossRef\]](#)
7. Chiu, P.W.; Phee, S.J.; Bhandari, P.; Sumiyama, K.; Ohya, T.; Wong, J.; Poon, C.C.Y.; Tajiri, H.; Nakajima, K.; Ho, K.Y. Enhancing proficiency in performing endoscopic submucosal dissection (ESD) by using a prototype robotic endoscope. *Endosc. Inter. Open* **2015**, *3*, 439–442. [\[CrossRef\]](#)
8. Hwang, M.; Kwon, D.S. K-FLEX: A flexible robotic platform for scar-free endoscopic surgery. *Inter. J. Med. Robot. Comput. Assist. Surg.* **2020**, *16*, e2078. [\[CrossRef\]](#)
9. Rayne, P.B.; Gras, G.; Leibrandt, K.; Wisanuvej, P.; Schmitz, A.; Seneci, C.A.; Yang, G.Z. The i^2 Snake robotic platform for endoscopic surgery. *Ann. Biomed. Eng.* **2018**, *46*, 1663–1675. [\[CrossRef\]](#)
10. Spaum, G.O.; Zheng, B.; Swanström, L.L. A multitasking platform for natural orifice transluminal endoscopic surgery (NOTES): A benchtop comparison of a new device for flexible endoscopic surgery and a standard dual-channel endoscope. *Surg. Endosc.* **2009**, *23*, 2720–2727. [\[CrossRef\]](#)
11. Abbott, D.J.; Becke, C.; Rothstein, R.I.; Peine, W.J. Design of an endoluminal NOTES robotic system. In Proceedings of the 2007 IEEE/RSJ International Conference on Intelligent Robots and Systems, IROS2007, San Diego, CA, USA, 29 October–2 November 2007; pp. 410–416.
12. Remacle, M.; Prasad, V.M.N.; Lawson, G.; Plisson, L.; Bachy, V.; van der Vorst, S. Transoral robotic surgery (TORS) with the Medrobotics FlexTM system: First surgical application on humans. *Eur. Arch. Otorhinolaryngol.* **2015**, *272*, 1451–1455. [\[CrossRef\]](#)

13. Lee, D.S.; Kim, J.W.; Lee, K.L.; Kim, B.G.; Kim, S.H.; Byeon, J.S. Technical feasibility of a newly designed bendable forceps for difficult endoscopic tissue samplings (with video). *Surg. Endosc.* **2020**, *34*, 4692–4701. [\[CrossRef\]](#)
14. Kawahara, T.; Matsumoto, T.; Muramatsu, N.; Osada, T.; Sakamoto, N.; Arai, F. Development of a decoupling wire driven exoskeletal microarm for endoscopic submucosal dissection. In Proceedings of the 3th IEEE RAS and EMBS International Conference on Biomedical Robotics and Biomechatronics, BioRob2010, Tokyo, Japan, 26–29 September 2010; pp. 849–854.
15. Prasai, A.B.; Jaiprakash, A.; Pandey, A.K.; Crawford, R.; Roberts, J.; Wu, L. Design and Fabrication of a Disposable Micro End Effector for Concentric Tube Robots. In Proceedings of the 14th International Conference on Control, Automation, Robotics and Vision, ICARCV2016, Phuket, Thailand, 13–15 November 2016.
16. Nakadate, R.; Nakamura, S.; Moriyama, T.; Kenmotsu, H.; Oguri, S.; Arata, J.; Uemura, M.; Ohuchida, K.; Akahoshi, T.; Ikeda, T.; et al. Gastric endoscopic submucosal dissection using novel 2.6-mm articulating devices: An ex vivo comparative and in vivo feasibility study. *Endoscopy* **2015**, *47*, 820–824. [\[CrossRef\]](#) [\[PubMed\]](#)
17. Okamoto, Y.; Nakadate, R.; Nakamura, S.; Arata, J.; Oguri, S.; Moriyama, T.; Esaki, M.; Iwasa, T.; Ohuchida, K.; Akahoshi, T.; et al. Colorectal endoscopic submucosal dissection using novel articulating devices: A comparative study in a live porcine model. *Surg. Endosc.* **2019**, *33*, 651–657. [\[CrossRef\]](#) [\[PubMed\]](#)
18. Nakadate, R.; Iwasa, T.; Onogi, S.; Arata, J.; Oguri, S.; Okamoto, Y.; Akahoshi, T.; Eto, M.; Hashizume, M. Surgical robot for intraluminal access: An ex vivo feasibility study. *Cyborg Bionic Syst.* **2020**, *2020*, 8378025. [\[CrossRef\]](#)
19. Ray, N.A.; Kwiat, D.; Rogers, S.; Lin, M.Y.C. Lowering the barrier of surgical endoscopy with a novel articulating retractor. *J. Med. Dev.* **2017**, *11*, 034501. [\[CrossRef\]](#)
20. Howell, L.L. *Compliant Mechanisms*; Wiley-Interscience: Hoboken, NJ, USA, 2001; ISBN 978-0-471-38478-6.
21. Runciman, M.; Darzi, A.; Mylonas, G.P. Soft robotics in minimally invasive surgery. *Soft Robot.* **2019**, *6*, 423–443. [\[CrossRef\]](#)
22. Jelinek, F.; Arkenbout, E.A.; Henselmans, P.W.J.; Pessers, R.; Breedveld, P. Classification of joints used in steerable instruments for minimally invasive surgery. *J. Med. Dev.* **2014**, *8*, 030914. [\[CrossRef\]](#)
23. Machekposhti, D.F.; Tolou, N.; Herder, J.L. A review on compliant joints and rigid-body constant velocity universal joints toward the design of compliant homokinetic couplings. *J. Mech. Des.* **2015**, *137*, 032301. [\[CrossRef\]](#)
24. Park, C.; Park, S.; Hong, H.; Jeon, I.H.; Kim, K. Development of an end-effector device for loose body removal in hip arthroscopy. *J. Eng. Med.* **2018**, *232*, 987–998. [\[CrossRef\]](#)
25. Wu, Z.; Bandara, D.S.V.; Kiguchi, K.; Arata, J. Design strategy for a surgical manipulator based on a compliant mechanism—Rigidity and range of motion: Finding the optimized balance. In Proceedings of the 2019 IEEE International Conference on Robotics and Biomimetics, ROBIO2019, Dali, China, 6–8 December 2019.
26. Huang, J.; Wang, H.; Tian, S.; Zhang, F. Modeling of notched variable stiffness continuum flexible snake-like robot. In Proceedings of the 2018 IEEE International Automatic Control Conference, CACS2018, Taoyuan, Taiwan, 4–7 November 2018.
27. Coemert, S.; Yalvac, B.; Bott, V.; Sun, Y.; Lueth, T. Development and validation of an automated FEM-based design optimization tool for continuum compliant structures. *Inter. J. Mech. Mat. Des.* **2020**, *17*, 245–269. [\[CrossRef\]](#)
28. Opatowski, J. Cantilever beams of uniform strength. *Quart. Appl. Math.* **1945**, *3*, 76–81. [\[CrossRef\]](#)
29. Suh, J.; Kim, K.; Jeong, J.; Lee, J. Design considerations for a hyper-redundant pulleyless rolling joint with elastic fixtures. *IEEE/ASME Trans. Mechatron.* **2015**, *20*, 2841–2852. [\[CrossRef\]](#)
30. Kim, K.; Woo, H.; Suh, J. Design and evaluation of a continuum robot with discretized link joints for cardiovascular interventions. In Proceedings of the 7th IEEE RAS and EMBS International Conference on Biomedical Robotics and Biomechatronics, BioRob2018, Enschede, The Netherlands, 26–29 August 2018; pp. 627–633.
31. Wang, Y.; Cao, Q.; Zhu, X.; Wang, P. A cable-driven distal end-effector mechanism for single-port robotic surgery. *Int. J. Comput. Assist. Radiol. Surg.* **2021**, *16*, 301–309. [\[CrossRef\]](#) [\[PubMed\]](#)
32. Ryu, S.C.; Renaud, P.; Black, R.J.; Daniel, B.L.; Cutkosky, M.R. Feasibility study of an optically actuated MR-compatible active needle. In Proceedings of the 2011 IEEE/RSJ International Conference on Intelligent Robots and Systems, IROS2011, San Francisco, CA, USA, 25–30 September 2011; pp. 2564–2569.
33. Swaney, P.J.; York, P.A.; Gilbert, H.B.; Kahrs, J.B.; Webster, R.J. Design, fabrication, and testing of a needle-sized wrist for surgical instruments. *J. Med. Dev.* **2017**, *11*, 014501. [\[CrossRef\]](#) [\[PubMed\]](#)
34. Eastwood, K.W.; Francis, P.; Azimian, H.; Swarup, A.; Looi, T.; Drake, J.M.; Naguib, H.E. Design of a constant-aided compliant notched-tube joint for surgical manipulation in confined workspaces. *J. Mech. Robot.* **2018**, *10*, 015001. [\[CrossRef\]](#)
35. Haga, Y.; Muyari, Y.; Goto, S.; Matsunaga, T.; Esashim, M. Development of minimally invasive medical tools using laser processing on cylindrical substrates. *IEEE Trans. Sens. Micromach.* **2008**, *128*, 402–409. [\[CrossRef\]](#)
36. Kutzner, M.D.M.; Segreti, S.M.; Brown, C.Y.; Taylor, R.H.; Mears, S.C.; Armand, M. Design of a New cable-driven manipulator with a large open lumen: Preliminary applications in the minimally-invasive removal of osteolysis. In Proceedings of the 2011 IEEE International Conference on Robotics and Automation, ICRA2011, Shanghai, China, 9–13 May 2011; pp. 2913–2920.
37. Gao, A.; Murphy, R.J.; Liu, H.; Iordachita, I.I.; Armand, M. Mechanical model of dexterous continuum manipulators with compliant joint and tendon/external force interactions. *IEEE/ASME Trans. Mechatron.* **2017**, *22*, 465–475. [\[CrossRef\]](#)
38. Chitalia, Y.; Jeong, S.; Bok, J.; Nguyen, V.; Melkote, S.; Chern, J.J.; Desai, J.P. Towards the design and development of a pediatric neuroendoscope tool. In Proceedings of the 2019 IEEE/RSJ International Conference on Intelligent Robots and Systems, IROS2019, Macau, China, 3–8 November 2019; pp. 2998–3004.

39. Chitalia, Y.; Deaton, N.J.; Jeong, S.; Rahman, N.; Desai, J.P. Towards fbg-based sensing for micro-scale and meso-scale continuum robots with large deflection. *IEEE Robot. Automat. Lett.* **2020**, *5*, 1712–1719. [[CrossRef](#)]
40. Chitalia, Y.; Jeong, S.; Deaton, N.; Chern, J.J.; Desai, J.P. Design and kinematics analysis of a robotic pediatric neuroendoscope tool body. *IEEE/ASME Trans. Mechatron.* **2020**, *25*, 985–995. [[CrossRef](#)]
41. Francis, P.; Eastwood, K.W.; Bodani, V.; Looi, T.; Drake, J.M. Design, modeling and teleoperation of a 2 mm diameter compliant instrument for the da Vinci platform. *Ann. Biomed. Eng.* **2018**, *43*, 1437–1449. [[CrossRef](#)] [[PubMed](#)]
42. Dearden, J.; Grames, C.; Orr, J.; Jensen, B.D.; Magleby, S.P.; Howell, L.L. Cylindrical cross-axis flexural pivots. *Precis. Eng.* **2018**, *51*, 604–613. [[CrossRef](#)]
43. Zhang, D.; Sun, Y.; Lueth, T. Design of a novel tendon-driven manipulator structure based on monolithic compliant rolling-contact joint for minimally invasive surgery. *Int. J. Comput. Assist. Radiol. Surg.* **2021**, *16*, 1615–1625. [[CrossRef](#)]
44. Hu, Y.; Zhang, L.; Li, W.; Yang, G.Z. Design and fabrication of a 3-D printed metallic flexible joint for snake-like surgical robot. *IEEE Robot. Autom. Lett.* **2019**, *4*, 1557–1563. [[CrossRef](#)]
45. Feng, F.; Hong, W.; Xie, L. Design of 3D-printed flexible joints with presettable stiffness for surgical robots. *IEEE Access* **2020**, *8*, 79573–79585. [[CrossRef](#)]
46. Culmone, C.; Henselmans, P.W.J.; van Starckenburg, R.I.B.; Breedveld, P. Exploring non-assembly 3D printing for novel compliant surgical devices. *PLoS ONE* **2020**, *15*, e0232952. [[CrossRef](#)]
47. Peirs, J.; Brussel, H.V.; Reynaerts, D.; Gersem, G.D. A flexible distal tip with two degrees of freedom for enhanced dexterity in endoscopic robot surgery. In Proceedings of the 13th Micromechanics Europe Workshop, MME2002, Sinaia, Romania, 6–8 October 2002; pp. 271–274.
48. Sun, Y.; Liu, Y.; Xu, L.; Zou, Y.; Faragasso, A.; Lueth, T. Automatic design of compliant surgical forceps with adaptive grasping functions. *IEEE Robot. Automat. Lett.* **2020**, *5*, 1095–1102. [[CrossRef](#)]
49. Sun, Y.; Zhang, D.; Liu, Y.; Lueth, T. FEM-based mechanics modeling of bio-inspired compliant mechanisms for medical applications. *IEEE Trans. Med. Robot. Bionics* **2020**, *2*, 364–373. [[CrossRef](#)]
50. Zhou, D.; Sanada, K.; Haraguchi, D. Robotic forceps with a flexible wrist joint made of super engineering plastic. *Sens. Mater.* **2020**, *32*, 1027–1039. [[CrossRef](#)]
51. Ugural, A.C.; Fenster, S.K. *Advanced Mechanics of Materials and Applied Elasticity*, 6th ed.; Pearson: London, UK, 2019.